Homobuffer thickness effect on the background electron carrier concentration of epitaxial ZnO thin films

Z. Yang,[1,a)] H. M. Zhou,[1] W. V. Chen,[2] L. Li,[1] J. Z. Zhao,[1] P. K. L. Yu,[2] and J. L. Liu[1,b)]
[1]*Department of Electrical Engineering, Quantum Structures Laboratory, University of California, Riverside, California 92521, USA*
[2]*Department of Electrical and Computer Engineering, University of California, San Diego, La Jolla, California 92093, USA*

(Received 16 May 2010; accepted 11 August 2010; published online 21 September 2010)

Epitaxial ZnO thin films were grown on *r*-plane sapphire substrates using plasma-assisted molecular-beam epitaxy. ZnO homobuffer layers grown at a lower temperature were introduced to improve the crystallinity of the top ZnO thin films. Thicker homobuffer layers lead to better crystallinity of the subsequent epitaxial ZnO thin films due to the strain relaxation effect. Residual background electron carrier concentration in these undoped ZnO thin films first decreases, then increases as the buffer layer thickness increases from ~1 to 30 nm, with a minimum electron concentration of $\sim 1 \times 10^{17}$ cm^{-3} occurring in ZnO homobuffer of ~5 nm. These results demonstrate that the optimized ZnO homobuffer thickness to achieve both good ZnO crystallinity and low residual electron concentration is determined by the relative electron carrier concentration ratios and mobility ratios between the buffer and epi-ZnO layers. © *2010 American Institute of Physics*. [doi:10.1063/1.3486445]

Undoped ZnO is "intrinsically" *n*-type with a residual "background" electron carrier concentration (n_r) ranging generally from 10^{14} to 10^{19} cm^{-3}, due to defects and impurity elements/complexes with very shallow donor levels, such as Zn_I (Zn interstitials),[1] H (hydrogen),[2] and Zn_I–N_O (N_O: N substitution of O).[3] The low n_r of an undoped ZnO is critically important,[4] for both fundamental studies and device applications. An effectively functional ZnO light emitting diode (LED) requires at least high 10^{17} to low 10^{18} cm^{-3} range hole concentration in the *p*-layer, based on the observation from GaN LEDs,[5] consequently n_r has to be optimized down to low 10^{17} cm^{-3} or below in undoped ZnO to lead to any reasonably reliable *p*-doping and optoelectronic devices. So far the record of lowest n_r in ZnO epitaxial thin films is on the order of 10^{15} to 10^{16} cm^{-3}.[4] Based on these ZnO films, breakthroughs in basic studies[6,7] and reliable devices[8–10] have been demonstrated. In short, optimization of undoped ZnO epitaxial thin films with minimized n_r is an indispensible step for ZnO *p*-doping and LED researches.

Toward this direction, we performed a systematic study of undoped ZnO epitaxial thin films grown on *r*-plane sapphire substrates using plasma-assisted molecular-beam epitaxy (MBE) with different homobuffer conditions. We chose *r*-plane sapphire as substrates, partially because it has a smaller lattice mismatch with ZnO than *c*-sapphire,[11] and semipolar *r*-plane substrates decrease the quantum confined Stark effect, which is desirable for future optoelectronic device applications.[12] Homobuffers are employed in our ZnO study, inspired from GaN research in earlier days[5] that homobuffers eventually substitute the heterobuffers, although heterobuffers have already made great success in ZnO.[13] As we kept other growth conditions the same and altered the homebuffer thickness, we observed that the crystallinity of the ZnO films improves with the increase in homobuffer thickness. However, n_r first decreases, then increases as the buffer thickness increases from ~1 to 30 nm with a minimum of n_r at ~5 nm thick homobuffer. This result is reasonable as the n_r in the buffer is much higher than that in the top epi-ZnO layer,[14,15] while the Hall measurements reflect the total effect of two layers.[14–18]

ZnO thin films were grown on *r*-plane sapphire substrates using plasma-assisted MBE. Zn and O sources were provided by a regular Knudsen-cell filled with elemental Zn (6N) and a radio frequency plasma source sustained with O_2 (5N) gas, respectively. A mass flow controller was used to precisely tune the O_2 flow rate. The ZnO homobuffer layers were grown at 550 °C, with 370 °C Zn cell temperature, 5.0 SCCM (standard cubic centimeter per minute at STP) O_2 gas flow rate, and 400 W oxygen plasma power for all samples. The top epi-ZnO layers were grown at 750 °C, with 360 °C Zn cell temperature, 5.0 SCCM O_2 gas flow rate, and 400 W oxygen plasma power for all samples. All the as-grown samples were *in situ* annealed at 850 °C in oxygen plasma for 20 min. The thickness of the buffer layer ranges from ~1 to 30 nm for samples B to G as shown in Table I. A reference sample A without buffer layer was also grown in the series for comparison. X-ray diffraction (XRD) measurements were performed in both θ-2θ and θ-ω (rocking curve) geometries. The scanning electron microscope (SEM) images were taken using a Philips XL30-FEG SEM. The atomic force microscope (AFM) images were taken using a Veeco Dimension 5000 AFM. Hall-effect measurements were carried out using a Quantum design physical properties measurement system at 300 K with various magnetic fields up to 10 T.

[a)]Present address: School of Engineering and Applied Sciences, Harvard University, MA 02138, USA.
[b)]Electronic mail: jianlin@ee.ucr.edu.

TABLE I. Homobuffer layer thickness, FWHM of XRC, and electron carrier concentration $n_{Overall}$ of samples A to G.

Sample no.	Homobuffer thickness (nm)	FWHM XRC (arc min)	$n_{Overall}$ (cm^{-3})
A	0	>300	1.03×10^{19}
B	~1	70.5	2.35×10^{18}
C	~3	66.3	3.49×10^{17}
D	~5	56.5	1.29×10^{17}
E	10	39.7	2.54×10^{18}
F	20	33.9	3.37×10^{18}
G	30	29.0	7.48×10^{18}

Figure 1(a) shows the XRD patterns of sample A in θ-2θ configuration. Besides the ZnO $(11\bar{2}0)$ peak (*a*-direction), two peaks from sapphire substrates are also observed due to the relatively small thickness of the film. It is common to get *a*-ZnO on *r*-sapphire (similar results have been reported elsewhere),[11,19–22] and whether the sapphire substrate peak show up[19,20] or not[21,22] depends on the top ZnO layer thickness. All other samples (B-F) show similar XRD patterns in θ-2θ geometry. In order to clarify the crystallinity of each sample, x-ray rocking curve (XRC) measurements were also performed on the samples A to G. The inset in Fig. 1(b) shows the XRC patterns of the ZnO $(11\bar{2}0)$ peaks in samples B and F. The black curves are the experimental data while the red and blue lines are the Gaussian fittings for samples B and F, respectively. The full-width-at-half-maximum (FWHM) values of the XRC curves are used to quantify the crystallinity of each sample. Figure 1(b) shows the plot of the FWHM of XRC versus homobuffer layer thickness of each sample. The data are also summarized in Table I. From Fig. 1(b), it is observed that thicker homobuffer layer leads to better crystallinity. When no buffer is employed in sample

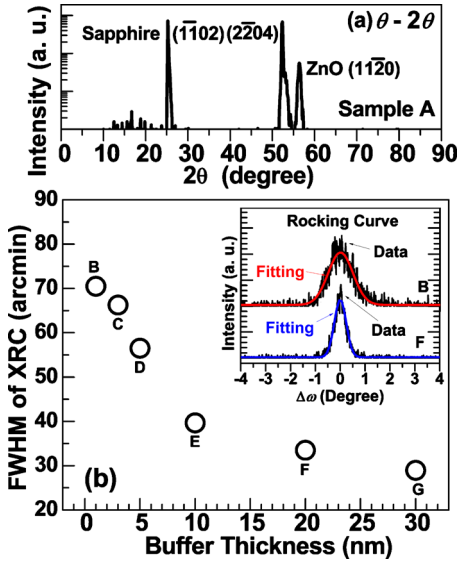

FIG. 1. (Color online) (a) XRD spectrum of sample A in θ-2θ geometry. (b) The plot of the FWHM of XRC vs homobuffer layer thickness. The inset in (b) shows the XRC patterns of the ZnO $(11\bar{2}0)$ peaks in samples B and F. The black curves are the experimental data while the red and blue lines are the Gaussian fittings for samples B and F, respectively.

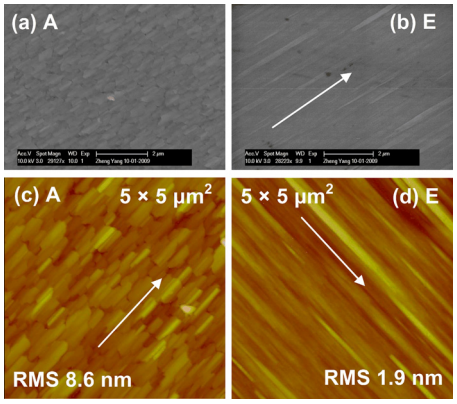

FIG. 2. (Color online) (a) and (b) SEM images of samples A and E. (c) and (d) AFM images of samples A and E in 5×5 μm^2 range. Without buffer layer, sample A shows the island growth mode, while sample E with homobuffer layer shows evident 2D growth mode. The arrows in (b), (c), and (d) show the *c*-direction of the ZnO.

A, the FWHM of the XRC is larger than 300 arc min. When the homobuffer thickness increases from ~1 to 30 nm, the FWHM of XRC decreases from 70.5 arc min in sample B to 29.0 arc min in sample G.

SEM and AFM studies were employed to clarify the surface morphology of the samples. Figures 2(a) and 2(b) show the SEM images of samples A and E. Without buffer layer, sample A shows the island growth mode, with columnar[23–25] islands along the *c*-direction, while sample E with homobuffer layer shows evident two-dimensional (2D) growth mode. The arrow in Fig. 2(b) indicates the *c*-direction of the ZnO film, which is perpendicular to the *a*-direction of the ZnO film plane. Figures 2(c) and 2(d) show the AFM images of samples A and E in 5×5 μm^2 range. The root-mean-square (rms) surface roughness of sample A is 8.6 nm. After homobuffer is introduced, the rms surface roughness of the ZnO thin film is significantly improved to be 1.9 nm for sample E. The arrows in the AFM images of Figs. 2(c) and 2(d) show the *c*-direction of ZnO.

Field-dependent Hall effect (from −10 to 10 T) was preformed on all the samples to measure the n_r of these undoped ZnO thin films. A linear fit was performed on the slope of the Hall resistance over the magnetic field, then this linear fit was used to calculate the electron carrier concentration.[26,27] The inset in Fig. 3 shows one example (sample B) that how the Hall effect was performed on each sample to obtain the electron carrier concentration. The electron concentrations are summarized in Table I. Figure 3 shows the plot of residual background electron carrier concentration versus homobuffer layer thickness. The minimum value of n_r occurs in sample D with a homobuffer thickness of ~5 nm. To understand this phenomenon, a two-layer effect needs to be considered during the Hall effect measurements under the frame of the following equation proposed by Look:[14,16–18]

$$n_{epi}=\frac{1}{d_{epi}}\frac{(n_{Overall}d_{Overall}\mu_{Overall}-n_{Buffer}d_{Buffer}\mu_{Buffer})^2}{n_{Overall}d_{Overall}\mu^2_{Overall}-n_{Buffer}d_{Buffer}\mu^2_{Buffer}}, \quad (1)$$

where, n_{Buffer}, μ_{Buffer}, and d_{Buffer} represent the electron carrier concentration, mobility, and thickness of the ZnO buffer

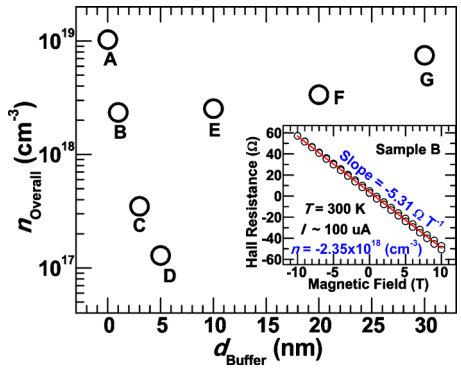

FIG. 3. (Color online) Plot of the overall residual background electron carrier concentration ($n_{Overall}$) vs homobuffer layer thickness (d_{Buffer}). The inset shows the approach (using sample B as an example) to obtain the electron carrier concentration, which performs a linear fit to the slope of the Hall resistance over the magnetic field (from −10 to 10 T) in the field dependent Hall effect.

layer; n_{epi} and d_{epi} represent the electron carrier concentration and thickness of the top epi-ZnO layer; and $n_{Overall}$, $\mu_{Overall}$, and $d_{Overall}$ represent the electron carrier concentration, mobility, and thickness of the total effect arising from two layers in the Hall effect. For example, in sample G, if the mobility $\mu_{Overall}=10$ cm^2/V s and total thickness is 100 nm (including 30 nm homobuffer), the mobility and electron carrier concentration of the buffer layer are $\mu_{Buffer}=9.74$ cm^2/V s and $n_{Buffer}=2.53\times10^{19}$ cm^{-3} (which can be obtained on a reference sample), respectively, the mobility and electron carrier concentration of the top epi-ZnO layer are $\mu_{epi}=32$ cm^2/V s and $n_{epi}=3.9\times10^{16}$ cm^{-3}, respectively. This means the better crystallinity as a result of thicker buffer layer can result in very good electronic property of top epi-ZnO layer (high mobility and low electron concentration), however, the poor electronic property of the thicker buffer underneath counteracts the good property of the epi-ZnO on top. The overall effect determines what the optimum buffer thickness is. Interestingly, similar results were also observed in GaN during its optimizations in earlier days, which partially leads to the breakthroughs in GaN light emitting devices subsequently.[5]

In summary, ZnO thin films were grown on *r*-sapphire using MBE. After low-temperature homobuffer was introduced, 2D growth mode of the top epi-ZnO layer was achieved. Thicker homobuffer layer results in better ZnO crystallinity. The residual background electron carrier concentration (n_r) in these ZnO thin films do not decrease monotonically with increased homobuffer thickness due to the larger n_r in the buffer layer, which affects the overall electronic properties of the top ZnO epilayer. The minimum n_r in this study occurs at ~5 nm thick buffer layer sample. The optimum buffer thickness (with minimum n_r) is determined by the ratio of the n_r and mobility between the homobuffer layer and top epi-ZnO layer.

This work was supported by DOE (Grant No. DE-FG02-08ER46520), by ARO-YIP (Grant No. W911NF-08-1-0432), by NSF (Grant No. ECCS-0900978), and by ONR/DMEA through the Center of Nanomaterials and Nanodevice (CNN) under the Award No. H94003-08-2-0803.

[1]D. C. Look, J. W. Hemsky, and J. R. Sizelove, Phys. Rev. Lett. **82**, 2552 (1999).
[2]S. F. J. Cox, E. A. Davis, S. P. Cottrell, P. J. C. King, J. S. Lord, J. M. Gil, H. V. Alberto, R. C. Vilão, J. Piroto Duarte, N. Ayres de Campos, A. Weidinger, R. L. Lichti, and S. J. C. Irvine, Phys. Rev. Lett. **86**, 2601 (2001).
[3]D. C. Look, G. C. Farlow, P. Reunchan, S. Limpijumnong, S. B. Zhang, and K. Norlund, Phys. Rev. Lett. **95**, 225502 (2005).
[4]A. Tsukazaki, A. Ohtomo, and M. Kawasaki, Appl. Phys. Lett. **88**, 152106 (2006).
[5]S. Nakamura, S. Pearton, and G. Fasol, *The Blue Laser Diode* (Springer, New York, 2000) S. Nakamura, Jpn. J. Appl. Phys., Part 2 **30**, L1705 (1991).
[6]A. Tsukazaki, A. Ohtomo, T. Kita, Y. Ohno, H. Ohno, and M. Kawasaki, Science **315**, 1388 (2007).
[7]A. Tsukazaki, H. Yuji, S. Akasaka, K. Tamura, K. Nakahara, T. Tanabe, H. Takasu, A. Ohtomo, and M. Kawasaki, Appl. Phys. Express **1**, 055004 (2008).
[8]T. I. Suzuki, A. Ohtomo, A. Tsukazaki, F. Sato, J. Nishii, H. Ohno, and M. Kawasaki, Adv. Mater. (Weinheim, Ger.) **16**, 1887 (2004).
[9]A. Tsukazaki, M. Kubota, A. Ohtomo, T. Onuma, K. Ohtani, H. Ohno, S. F. Chichibu, and M. Kawasaki, Jpn. J. Appl. Phys., Part 2 **44**, L643 (2005).
[10]A. Tsukazaki, A. Ohtomo, T. Onuma, M. Ohtani, T. Makino, M. Sumiya, K. Ohtani, S. F. Chichibu, S. Fuke, Y. Segawa, H. Ohno, H. Koinuma, and M. Kawasaki, Nature Mater. **4**, 42 (2005).
[11]Ü. Özgür, Ya. I. Alivov, C. Liu, A. Teke, M. A. Reshchikov, S. Doğan, V. Avrutin, S.-J. Cho, and H. Morkoç, J. Appl. Phys. **98**, 041301 (2005).
[12]A. Tyagi, Y. D. Lin, D. A. Cohen, M. Saito, K. Fujito, J. S. Speck, S. P. Denbaars, and S. Nakamura, Appl. Phys. Express **1**, 091103 (2008).
[13]X. Du, Z. Mei, Z. Liu, Y. Guo, T. Zhang, Y. Hou, Z. Zhang, Q. Xue, and A. Y. Kuznetsov, Adv. Mater. (Weinheim, Ger.) **21**, 4625 (2009).
[14]D. C. Look and R. J. Molnar, Appl. Phys. Lett. **70**, 3377 (1997).
[15]L. Li, C. X. Shan, S. P. Wang, B. H. Li, J. Y. Zhang, B. Yao, D. Z. Shen, X. W. Fan, and Y. M. Lu, J. Phys. D: Appl. Phys. **42**, 195403 (2009).
[16]D. C. Look, *Electrical Characterization of GaAs Materials and Devices* (Wiley, New York, 1989).
[17]D. C. Look, H. L. Mosbacker, Y. M. Strzhemechny, and L. J. Brillson, Superlattices Microstruct. **38**, 406 (2005).
[18]D. C. Look, Superlattices Microstruct. **42**, 284 (2007).
[19]F. X. Xiu, Z. Yang, L. J. Mandalapu, J. L. Liu, and W. P. Beyermann, Appl. Phys. Lett. **88**, 052106 (2006).
[20]Z. Yang, J. H. Lim, S. Chu, Z. Zuo, and J. L. Liu, Appl. Surf. Sci. **255**, 3375 (2008).
[21]Z. Yang, J. L. Liu, M. Biasini, and W. P. Beyermann, Appl. Phys. Lett. **92**, 042111 (2008).
[22]Z. Yang, D. C. Look, and J. L. Liu, Appl. Phys. Lett. **94**, 072101 (2009).
[23]J. Kong, S. Chu, M. Olmedo, L. Li, Z. Yang, and J. L. Liu, Appl. Phys. Lett. **93**, 132113 (2008).
[24]S. Chu, M. Olmedo, Z. Yang, J. Kong, and J. L. Liu, Appl. Phys. Lett. **93**, 181106 (2008).
[25]Z. Yang, S. Chu, W. V. Chen, L. Li, J. Kong, J. Ren, P. K. L. Yu, and J. L. Liu, Appl. Phys. Express **3**, 032101 (2010).
[26]Z. Yang, M. Biasini, W. P. Beyermann, M. B. Katz, O. K. Ezekoye, X. Q. Pan, Y. Pu, J. Shi, Z. Zuo, and J. L. Liu, J. Appl. Phys. **104**, 113712 (2008).
[27]Z. Yang, W. P. Beyermann, M. B. Katz, O. K. Ezekoye, Z. Zuo, Y. Pu, J. Shi, X. Q. Pan, and J. L. Liu, J. Appl. Phys. **105**, 053708 (2009).